PAPER 17

Prediction of the microstructure of submerged arc linepipe welds

H.K.D.H. Bhadeshia, BSc, PhD(Cantab), CEng, L.E. Svensson, MSc, PhD and B. Gretoft

SUMMARY

An important factor controlling the toughness of steel weld deposits is the primary microstructure. Recent theoretical work has indicated that this microstructure can be rationalised with the help of phase transformation theory, and the theory has been used to predict successfully the microstructure of Fe-C-Si-Mn and Fe-C-Si-Mn-Ni manual metal arc welds. In this work we report the application of this theory to longitudinal two-pass submerged arc Fe-C-Si-Mn and Fe-C-Si-Mn-Mo welds. The results are compared with new experimental results and with mechanical property data.

INTRODUCTION

There are so many variables involved in the production of a successful arc-weld deposit that the design of welding consumables and procedures can be extremely complicated, expensive and time-consuming. For the off-shore industry, much of the design effort is of course aimed at producing weld deposits with ever increasing toughness and strength combinations. One of the principal factors influencing these mechanical properties is the as-deposited (or primary) microstructure of the weld, a function of the detailed weld chemistry and of the welding conditions. Considerable work (1-7) has recently been done towards the prediction of this microstructure using phase transformation theory. For example, it is now established that the primary microstructure of manual metal arc low-alloy steel welds containing C, Mn, Si and Ni in any combination can be estimated fairly accurately as a function of welding conditions and joint geometry; computer software (5) has been developed to enable the necessarily complicated calculations to be carried out on a routine basis. In this work, we attempt to apply the model for the prediction of microstructure to longitudinal, two-pass tandem submerged arc welds of the type used for pipeline welding. The model is tested against experimental data from Fe-C-Si-Mn and Fe-C-Si-Mn-Mo deposits and mechanical property data from these welds are also reported.

EXPERIMENTAL

The weld geometry is illustrated in Fig. 1, the double-Y preparation being typical of pipe welds; we note that this preparation does imply a considerable dilution of the weld metal by the base plate. The welds were produced by tandem submerged arc welding, as illustrated in Fig. 2. For the bottom bead (deposited first), the welding conditions were 1000A, 30V(DC+), 2.36mm/s for the leading electrode and 625A, 38V(AC) for the trailing electrode. For the top bead, the welding conditions were 950A, 31V(DC+) 2.5mm/s for the leading electrode and 625A, 38V(AC) for the trailing electrode. Both electrodes were 4mm in diameter; all the electrodes used in this study are experimental electrodes. A basic, agglomerated flux (proprietary designation OK 10.71, basicity 1.6, density 1.1kg/l) was used for all the experiments. The interpass temperature was 100°C. The compositions of the welds and of the base plate are given in Table 1.

Optical microscopy was carried out on transverse sections of the welds; the microstructural measurements were all carried out on the top run, using a Swift

point counter (magnification x500) with at least 500 points per weld. Lineal intercept measurements were carried out on a Quantimet 720 image analysing computer, using tracings of γ grain structure from montages of micrographs taken at x100 magnification. Edge errors arising during measurements were completely avoided by using a guard region. The weld cooling curves were measured as discussed in Ref. 1, 4.

Standard Charpy impact tests were carried out at 20, 0, -20, -40 and -60°C with five tests at each temperature. Tensile tests (two per weld) were carried out on each weld using 4mm diameter specimens; elongation was measured on a 20mm gauge length.

Table 1 Compositions of experimental weld deposits and of the base plate. The concentrations are in wt.%, except B, O and N which are in ppm by wt. The concentration of Ti is in all cases less than 0.001 wt.%. The concentrations of Pb, Sn, As, Sb and V are in all cases less than 0.007 wt.%.

	Weld 1	Weld 2	Weld 3	Weld 4	Base Plate
C	0.14	0.14	0.14	0.13	0.17
Si	0.29	0.24	0.31	0.27	0.22
Mn	1.44	1.54	1.32	1.60	1.65
Mo	0.01	0.19	0.24	0.39	0.04
Ni	0.06	0.03	0.03	0.04	0.03
Cr	0.05	0.03	0.03	0.04	0.04
Al	0.013	0.018	0.017	0.018	0.007
P	0.029	0.027	0.028	0.025	0.031
S	0.006	0.029	0.006	0.027	0.005
O	424	489	442	465	105
N	97	103	82	110	77
B	4	4	5	4	5

THEORY FOR THE PREDICTION OF THE MICROSTRUCTURE

The flow-diagram presented in Fig. 3 illustrates the overall path followed for the calculations; to save space, detailed references are not stated but are listed in (1). The morphology of the γ grains in the primary microstructure can be represented as a honeycomb of hexagonal prisms, the side length of each prism being 'a' and the length of the prism being 'c' (1,9). The c-axes of these prisms are approximately parallel to the direction of maximum heat flow during solidification; if $\bar{L}_{tn}$ is the mean lineal intercept measured on a transverse section of the weld, in a direction normal to the major axes of the γ grains, then

$$\bar{L}_{tn} = \pi a \cos(30^{\circ})/2, \qquad [1]$$

so that 'a' can be determined experimentally (1,9). The parameter 'c' is not needed for the microstructure calculations because c>>a so that any effect due to the ends of the hexagonal prisms can be neglected. On further cooling, at $T=T_h$, the γ begins to transform, to layers of allotriomorphic ferrite (α) which grow by a diffusional transformation mechanism, at the γ/γ boundaries. As the temperature falls, diffusional growth becomes more difficult and Widmanstätten ferrite (α_w) plates nucleate at the α/γ boundaries and grow into the γ by a displacive transformation mechanism, at a rate controlled approximately by the diffusion of C in the γ ahead of the plate tips. At the same time, acicular ferrite (α_a) nucleates on inclusions (10), and also by autocatalytic effects (11), within the γ grains and grows in the form of thin plates. As the M_s temperature is approached, the small amount of remaining austenite decomposes either into degenerate pearlite and/or mixtures of martensite and retained austenite; because the volume fraction of these phases is relatively small,

they are called "microphases".

T_h is determined by using an additive reaction rule, the cooling curve and a computed Time-Temperature-Transformation (TTT) diagram for the alloy concerned. The TTT diagram consists of two 'C' curves, the upper one giving the time for the isothermal initiation of diffusional transformations such as α and pearlite, while the lower C curve represents the initiation times for displacive transformations such as α_w, α_a and bainite (10). The cross-over point of the two C curves is the temperature T_1 below which displacive transformations are assumed to be kinetically favoured, so that the growth of α ceases and gives way to α_w and α_a formation. In the temperature range T_h-T_1, the α layers at the γ/γ boundaries are assumed to thicken by a paraequilibrium mechanism, at a rate controlled by the diffusion of carbon in the γ ahead of the moving α/γ interface. During isothermal transformation at a temperature T, the half-thickness of each such layer is given by:

$$q = \alpha_1 t^{1/2} \qquad [2]$$

where α_1 is called the one-dimensional parabolic thickening rate constant, obtained by solving

$$\{2(x^{\gamma\alpha}-\bar{x})/(x^{\gamma\alpha}-x^{\alpha\gamma})\}\{(\underline{D}/\pi)^{1/2}\} = \alpha_1\{\exp[\alpha_1^2/(4\underline{D}/\pi)]\}\{1-\mathrm{erf}[\alpha_1/2\underline{D}^{1/2})]\} \qquad [3]$$

and t is the time, defined to be zero when q=0. $x^{\alpha\gamma}$ and $x^{\gamma\alpha}$ are the paraequilibrium carbon concentration of α and of γ respectively, calculated as in Ref. 1. The diffusion coefficient D of carbon in γ is a sensitive function of the carbon concentration in austenite (x_γ). Throughout this work, D is expressed as a function of concentration and temperature using Siller and McLellans theory as discussed in Ref. 1. Since x_γ varies with distance ahead of the α/γ interface, a weighted average diffusion coefficient $\underline{D}$ is used in equation 2, and is defined as

$$\underline{D} = \int_{x^{\gamma\alpha}}^{\bar{x}} D\, dx/(\bar{x} - x^{\gamma\alpha}). \qquad [4]$$

Although this equation is strictly only valid for steady-state growth, Coates (12) has suggested that it should be a reasonable approximation for parabolic growth as well, although he did not justify this. To check the level of approximation involved, all the parabolic rate constants used in this work were calculated in two ways: the first method used the approximation that eq. 4 is applicable to parabolic growth. The second more rigorous calculation is based on Atkinson's iterative (13) procedure for the numerical solution of the diffusion equation for one-dimensional diffusion-controlled growth; this allows the calculation of a rate constant α_1, for thickening in which the diffusion coefficient is a function of concentration. A comparison of the rate constants obtained by the two methods is given in Fig. 4, which shows very good agreement between the two methods, indicating that eq. 4 is a reasonable approximation to the problem.

Since the α grows anisothermally during cooling of the weld deposit, q is actually obtained by numerically integrating the function

$$q = \int_{t=0}^{t=t_1} 0.5\alpha_1\, t^{-0.5}\, dt \qquad [5]$$

where t_1 is the time taken for the weld deposit to cool from T_h to T_1. Here, the parabolic rate constant is a function of time and temperature. The volume fraction v_α of α is then derived as a function of a and q:

$$v_\alpha = [4qC_3(a-2qC_3)/a^2] \quad [6]$$

where $C_3=\tan(30^\circ)$. A better fit is obtained by empirically correcting this to give a corrected volume fraction V_α (and this gives a corresponding corrected value of allotriomorph thickness q') where

$$V_\alpha = 2.04v_\alpha + 0.035, \quad [7]$$

the calculated value thus being smaller than the actual value by a factor of $\sim$2, although the correlation between v_α and the actual volume fraction of α is typically found to be 0.95 (1).

At $T=T_1$, α_w formation begins, but the growth rate of α_w in welds is generally so high that growth ceases within a fraction of a second, and α_w formation can therefore be considered to occur isothermally at T_1. However, the volume fraction v_w of Widmanstätten ferrite in general correlates badly with its lengthening rate (G); impingement with acicular ferrite has to be taken into account. If the time available for unhindered α growth is t_2, then v_w is given by:

$$v_w = 3.34G(a-2q'C_3)t_2^2/a^2 \quad [8]$$

G is calculated for $T=T_1$, by the method described in (1). In the absence of impingement with α_a, the time available for α_w to grow right across the γ grains is t_3, given by:

$$t_3 = 2[a\sin(60^\circ) - q']/G \quad [9]$$

If t_3 is less than a critical time t_c, then α_w can grow without impingement with acicular ferrite and t_2 in Eq. (9) is set to equal t_3. On the other hand, if $t_c<t_3$ than α_w growth is terminated by impingement with α_a, and t_2 is set equal to t_c. t_c is experimentally found to be 0.21s for welds containing inclusions which nucleate acicular ferrite; although t_c is not sensitive to oxygen concentration, it is recognised that it may vary, depending on the ability of inclusions to nucleate acicular ferrite. The microphase volume fraction v_m can also be estimated thermodynamically, so that:

$$v_a = 1 - V_\alpha - v_w - v_m \quad [10]$$

where v_a is the volume fraction of α_a. It is usual to include the microphases in the v_w and v_a measurements, since v_m is generally small; hence, microphases are not measured or calculated separately in this work.

The high cooling rates associated with arc welding inevitably lead to solute segregation during solidification. The biggest effect of such segregation is to alter T_h (3); the details are given in (3).

RESULTS AND DISCUSSION

Cooling curves

Cooling curves obtained by harpooning thermocouples into the weld pool, during the deposition of the top beads of welds 1 and 3 are presented in Fig. 5; they were found to be virtually identical for the two welds. In order to calculate the microstructure, it is necessary to express the cooling rate as a function

of temperature and welding conditions. If it is assumed that the cooling rate is approximately independent of the position in the fusion zone of the weld, then it can be represented empirically by the equation

$$dT/dt = (C_1(T-T_i)^{C_2})/(Q\eta) \qquad [12]$$

where Q is the electrical energy input in units of J/m, η is the arc transfer efficiency, taken to be 0.95; for submerged arc processes, η is known to be high. T and T_i represent the temperature and the interpass temperature respectively (in ^{o}C), and t is the time in seconds. This equation has some justification in Rosenthal's theory for three-dimensional heat flow with a moving point heat source, but its use in the present context cannot be justified in detail; the equation is nevertheless found to be suitable for the fusion zone if the constants C_1 and C_2 are treated as adjustable parameters to be deduced by fitting to experimental data (4). For the cooling curves of Fig. 5, the cooling rate over the temperature range 800-400^{o}C is well represented by Eq. 12 with C_1=1.076 and C_2=2.6798. The standard error for the regression constant $\{[\ln(C_1)]$= -14.51$\}$ in a plot of $\ln[(dT/dt)Q\eta]$ versus $\ln(T-T_i)$, for all the data of Fig. 5, was found to be 0.83, and the standard error for the regression coefficient C_2 was found to be 0.13, the correlation coefficient for the plot being 0.99.

Microstructure

Fig. 6 shows the microstructure of weld 1; it consists of allotriomorphic ferrite, Widmanstätten ferrite and acicular ferrite together with microphases. The polycrystalline layers of allotriomorphic ferrite cover the $\gamma\gamma$ boundaries fairly uniformly. The lengthening of the plates of Widmanstätten ferrite is clearly seen to be limited by hard impingement with intragranularly nucleated acicular ferrite. An essential difference between weld 1 and the Mo containing welds (typical microstructure in Fig. 7) is that the allotriomorphic ferrite layers were found to be discontinuous in the latter welds. It was therefore very difficult to identify reliably the austenite grain boundaries in welds 2-4, especially at the low magnifications needed for the measurements. The grain size measurements could only be conducted on samples of weld 1, where '2a' was found to be 96μm; this grain size was then assumed to be applicable to all the welds, irrespective of Mo content, for the purposes of microstructure calculation.

Quantitative microstructural data are presented in Table 2; Fig. 8 illustrates how the Time-Temperature-Transformation (TTT) curve of a weld is influenced by solidification-induced segregation of substitutional alloying elements. The main effect is to raise the temperature T_h at which allotriomorphic ferrite first forms during continuous cooling. Fig. 9 shows that the agreement between the calculated and experimental microstructural data is reasonable, although in the case of Mo containing welds, the theory overestimates V_α, the error in general increasing with Mo content. This is consistent with the fact that the theory assumes the presence of continuous layers of α at the austenite grain boundaries. With the Mo containing welds, the α does not actually site-saturate the austenite grain boundaries, the α allotriomorphs being discontinuous. This must lead to an overestimation of V_α, as is observed. The problem cannot as yet be theoretically resolved since much detailed work needs to be done on the grain boundary nucleation of allotriomorphic ferrite. We also note that some of the error in the case of the Mo containing welds may be attributable to the lack of accurate γ grain size values.

Welds 2 and 4 have unusually high volume fractions of Widmanstatten ferrite and the reason for this is not obvious. In spite of these difficulties, the amount of acicular ferrite is predicted well. This is because of the relatively high

carbon and alloy content (the former being more important) of the welds, which in turn reduces the volume fractions of α and α_w. Consequently, any errors in V_α and v_w are themselves, on an absolute scale, relatively small and have a small effect on the calculated volume fraction of acicular ferrite. Finally, we see from Table 2 that the values of t_2 are consistent with the observation (Fig. 5,6) that the lengthening of Widmanstätten ferrite is limited by hard impingement with intragranularly nucleated acicular ferrite.

Table 2 Quantitative microstructural and mechanical property data.

	Weld 1	Weld 2	Weld 3	Weld 4
V_α	0.30	0.19	0.12	0.13
v_w	0.11	0.24	0.12	0.22
v_a	0.59	0.57	0.76	0.65
V_α calculated	0.28	0.27	0.32	0.29
v_w calculated	0.05	0.04	0.06	0.05
v_a calculated	0.67	0.69	0.62	0.65
t_2, s, calculated	0.211	0.211	0.211	0.211
Yield Stress, MPa	577	582	612	606
UTS, MPa	661	697	712	706
Elongation %	27	26	26	22
Reduction of Area %	66	63	64	64

Mechanical Properties

Weld 3, which has the smallest amount of allotriomorphic ferrite and the highest amount of acicular ferrite also has the best toughness (Fig. 10) even though its yield stress is above that of any other weld. This is consistent with the idea that it is the thickness of the layer of α which, along with the nature of inclusions, controls the toughness of welds, and with the notion that acicular ferrite is the desired phase for toughness. Of course, v_α and v_a are not entirely independent variables, but it seems more important to restrict the thickness of α, which really is the weaker phase. It is important to note that the α thickness can vary independently of v_α since the latter also depends on the austenite grain size. The welds all contain approximately the same amounts of inclusion forming elements, so that the above comparisons are valid, as long as the inclusion size distributions are similar.

Further Calculations

The results indicate that the microstructure of pipe welds produced by tandem submerged arc welding can be estimated using the model described earlier. However, more work is needed to account for the presence of discontinuous layers of ferrite at the austenite grain boundaries, as is the case for the Mo containing welds. The model can nevertheless be used to predict the effects of C, Si, Mn and elements such as Ni, and some illustrative calculations are presented in Fig. 11.

CONCLUSIONS

It has been shown that phase transformations theory can be used to estimate the microstructure of submerged arc welds for pipeline welding applications. For welds where the composition and cooling conditions are such that the austenite grain boundaries are not fully decorated with layers of allotriomorphic ferrite, more work is necessary before the microstructure can be estimated accurately. Particular attention needs to be paid to the kinetics of grain boundary nucleation.

REFERENCES

1. Bhadeshia H K D H, Svensson L E and Gretoft B: 'A Model for the Development of Microstructure in Low-Alloy Steel Welds' Acta Metall. 1985 33 1271-1283.
2. Bhadeshia H K D H, Svensson L E and Gretoft B: 'Influence of Alloying Elements on the formation of Allotriomorphic Ferrite in low-alloy steel weld deposits' J. Mat. Sci. Let 1985 4 305-308.
3. Gretoft B, Bhadeshia H K D H and Svensson L E: 'Development of Microstructure in the Fusion Zone of Steel Weld Deposits' Acta Stereologica', in press.
4. Svensson L E, Gretoft B and Bhadeshia H K D H: 'An analysis of cooling curves from the fusion zone of steel weld deposits' Scand. J. of Metallurgy 1986 15 97-103.
5. Svensson L E, Gretoft B and Bhadeshia H K D H: 'Computer-aided design of electrodes for MMA welding 'Proceedings of WI conference on Computer Technology in Welding, 1986, in press.
6. Bhadeshia H K D H, Svensson L E and Gretoft B: 'Prediction of Microstructure in the Fusion Zone of Multicomponent Steel Weld Deposits', Proc. of Int. Conf. on Trends in Welding Research, 1986, in press.
7. Yang J R and Bhadeshia H K D H: 'Thermodynamics of the Acicular Ferrite Transformation in Alloy-Steels Welds', Proc. of Int. Conf. on Trends in Welding Research, 1986, in press.
8. Strangwood M and Bhadeshia H K D H: 'Mechanism of Acicular Ferrite formation in Steel Weld Deposits, Proc. of Int. Conf. on Trends in Welding Research, 1986, in press.
9. Bhadeshia H K D H, Svensson L E and Gretoft B: 'The Austenite Grain Structure of low-alloy Steel Weld Deposits', J. Mat. Sci., in press.
10. Ito Y and Nakanishi M: 'Study on Charpy impact properties of weld metal with submerged arc welding', Sumitomo Search 1976 (15).
11. Barritte G, Ricks R and Howell P R: 'Application of STEM/EDS to study of microstructural development in HSLA steel weld metals', Quantitative Microanalysis with High Spatial Resolution, published by the Metals Society, London, 1981 p. 112.
12. Coates D E: 'Diffusional Growth Limitation and Hardenability', Metall. Trans. 1973 4 2313-2325.
13. Atkinson C: 'Numerical solutions to Planar Growth where the Diffusion Coefficient is Concentration Dependent', Acta Metall. 1967 16 1019-1022.

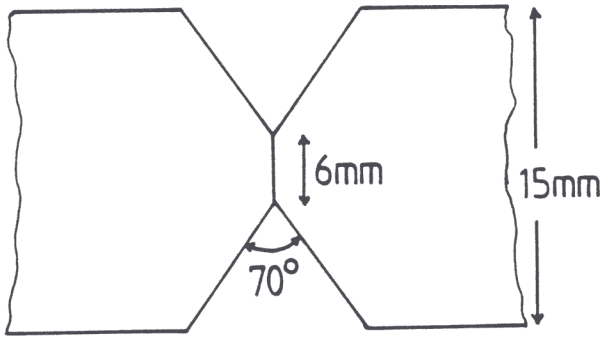

1 Weld Geometry

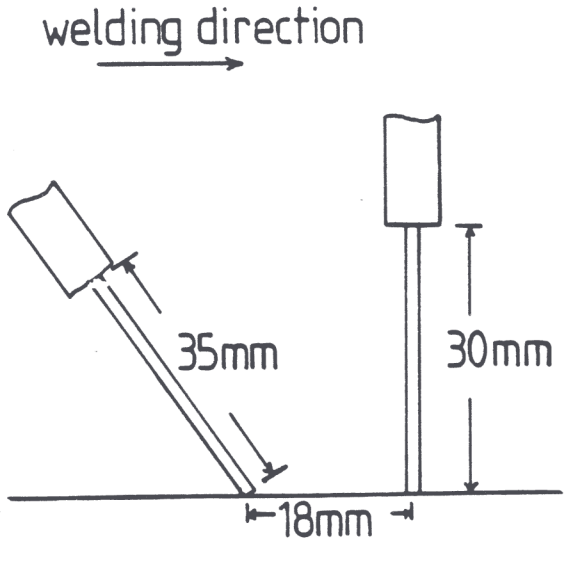

2 Welding Process

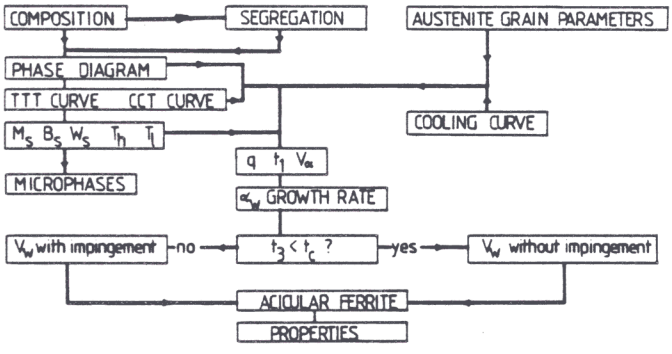

3 Flow chart illustrating the steps in the calculation of microstructure.

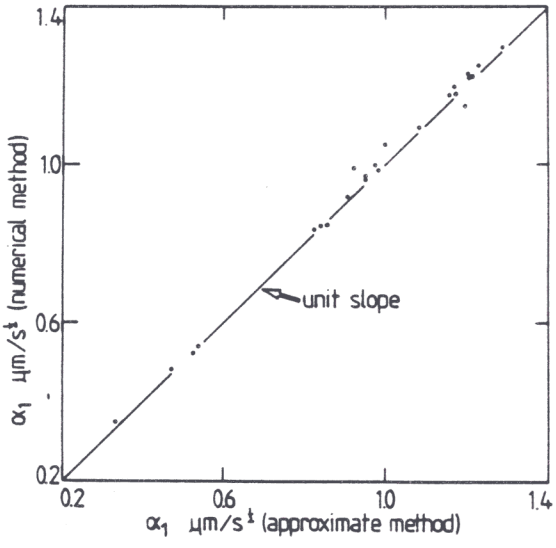

4 Comparison of the parabolic rate constants calculated using the two methods discussed in the text.

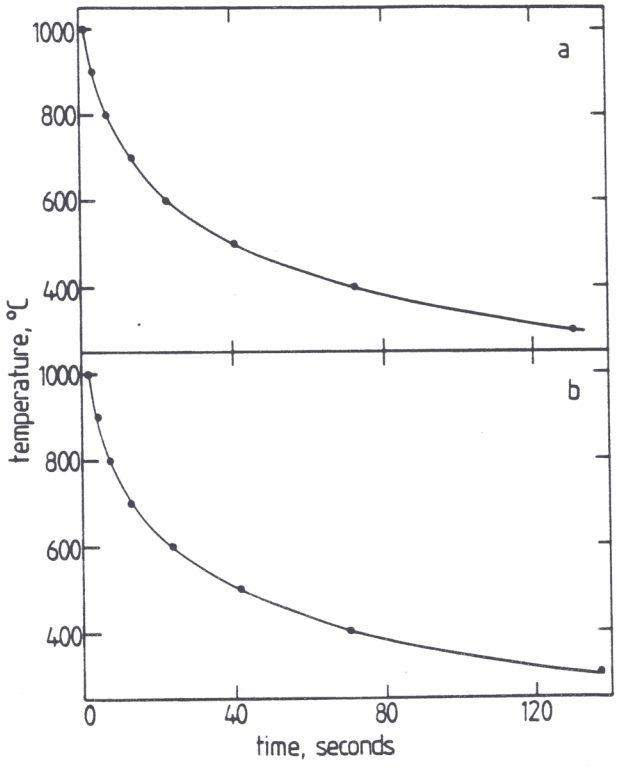

5 Experimental cooling curves: a) Weld 1, b) Weld 3.

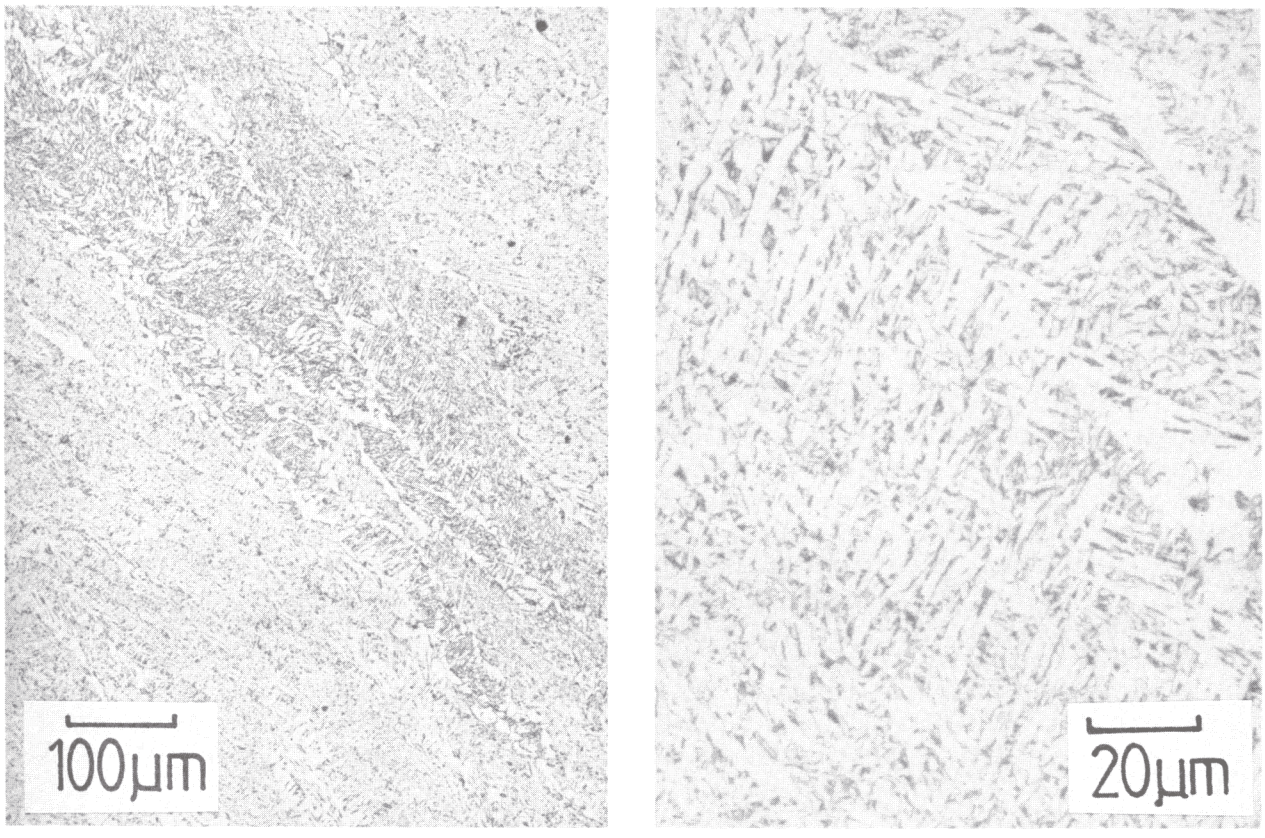

6 Optical micrographs from the fusion zone of Weld 1.

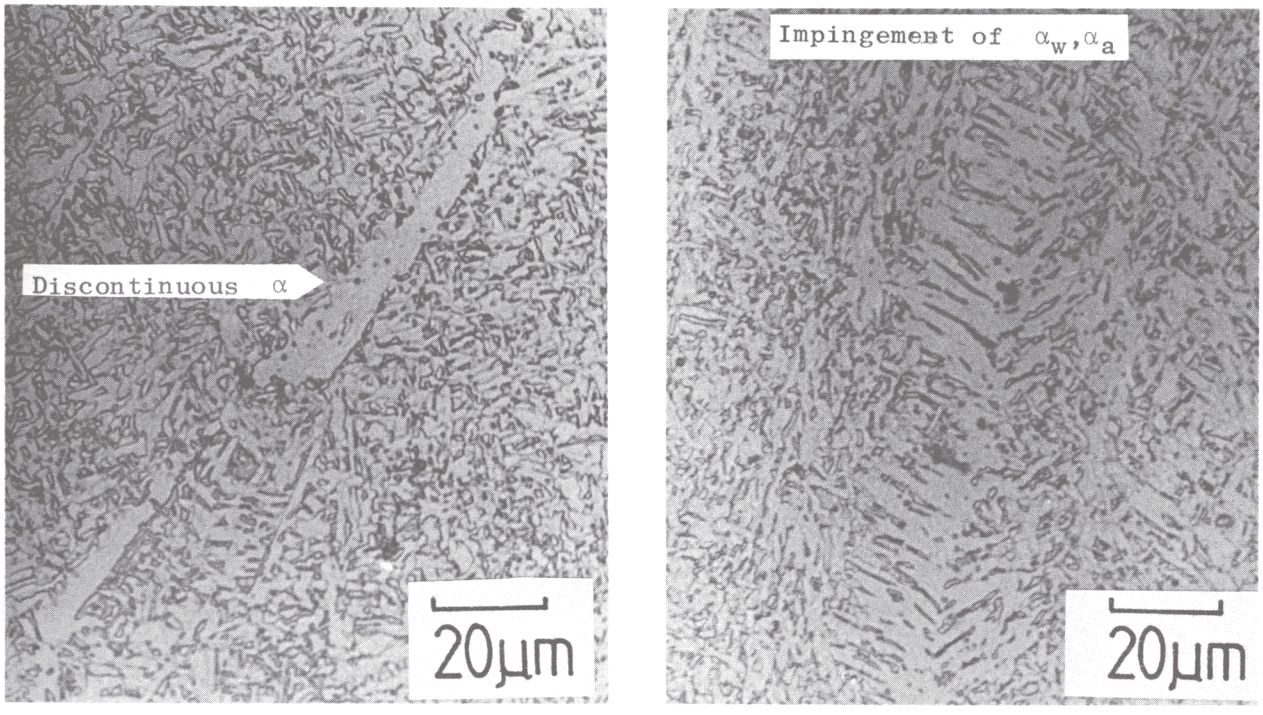

7 Optical micrographs from the fusion zone of Weld 4.

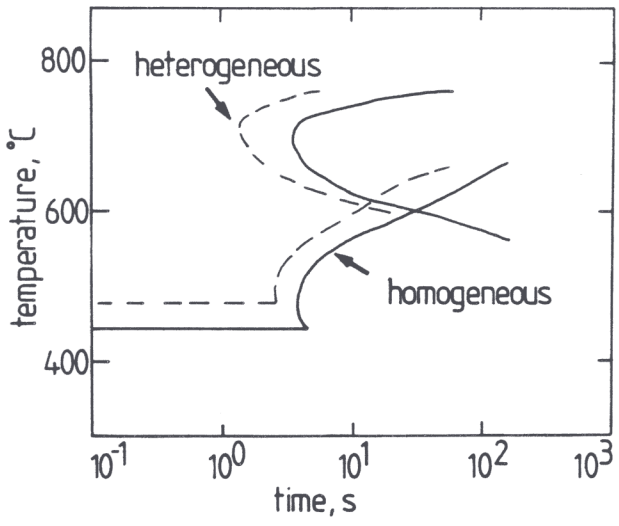

8 TTT curves showing the effect of segregation in accelerating kinetics.

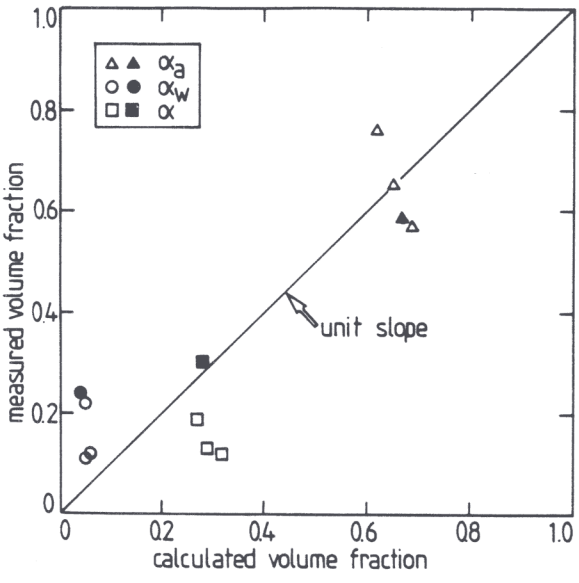

9 Comparison of calculated and experimental volume fractions. Filled points represent Weld 1.

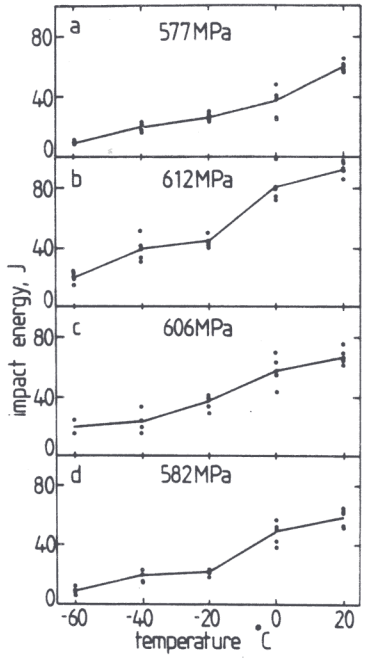

10 Charpy impact tests for welds 1, 3, 2 and 4 respectively

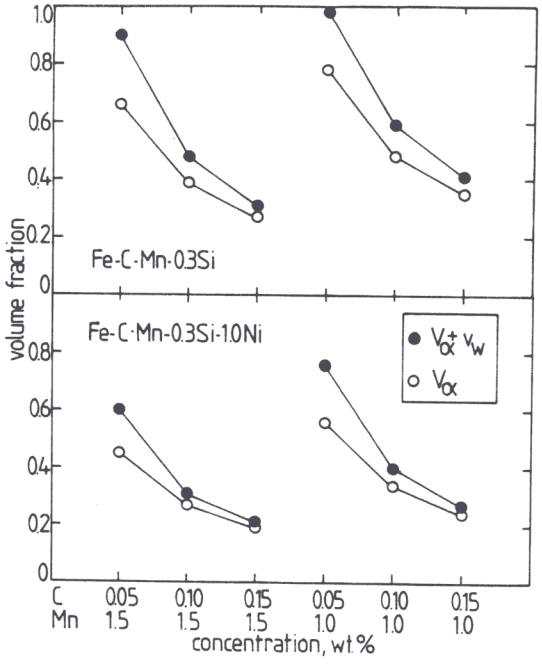

11 Calculations of weld microstructure

Third International Conference on
WELDING AND PERFORMANCE OF PIPELINES

London, 18-21 November 1986

P.H.M. HART

Conference Technical Director

Preprints

Part 1

The Welding Institute
Abington Hall, Abington, Cambridge CB1 6AL